Role of dimensionality in the Kondo CeTX_2 family: The case of CeCd$_{0.7}$Sb$_2$

P. F. S. Rosa,[1,2] R. J. Bourg,[1] C. B. R. Jesus,[2] P. G. Pagliuso,[2] and Z. Fisk[1]

[1]*University of California, Irvine, California 92697-4574, USA*
[2]*Instituto de Física "Gleb Wataghin", UNICAMP, Campinas-SP, 13083-859, Brazil*

Motivated by the presence of competing magnetic interactions in the heavy fermion family CeTX_2 (T = transition metal, X = pnictogen), here we study the novel parent compound CeCd$_{0.7}$Sb$_2$ by combining magnetization, electrical resistivity, and heat-capacity measurements. Contrary to the antiferromagnetic (AFM) ground state observed in most members of this family, the magnetic properties of our CeCd$_{0.7}$Sb$_2$ single crystals revealed a ferromagnetic ordering at T_c = 3 K with an unusual soft behavior. By using a mean field model including anisotropic nearest-neighbor interactions and the tetragonal crystalline electric field (CEF) Hamiltonian, a systematic analysis of our macroscopic data was obtained. Our fits allowed us to extract a simple but very distinct CEF scheme, as compared to the AFM counterparts. As in the previously studied ferromagnet CeAgSb$_2$, a pure $|\pm 1/2\rangle$ ground state is realized, hinting at a general trend within the ferromagnetic members. More generally, we propose a scenario for the understanding of the magnetism in this family of compounds based on the subtle changes of dimensionality in the crystal structure.

I. INTRODUCTION

A rich variety of ground states emerges in heavy fermion compounds due to the competition between Ruderman-Kittel-Kasuya-Yosida (RKKY) magnetic interactions, on-site Kondo interactions, and crystalline electrical field (CEF) effects [1]. In particular, tetragonal Ce-based compounds host numerous interesting phenomena as a result of such interplay. For instance, heavy fermion superconductivity is observed in CeCu$_2$Si$_2$ and CeTIn$_5$ (T = Co, Rh) and complex antiferromagnetism (AFM) with multiple field-induced transitions can be found in CeAgBi$_2$ and CeAuSb$_2$ [2–8]. The distance between Ce moments, i.e., the lattice parameter a, commonly found in these compounds ranges from 4 to 5 Å. Since nearest-neighbor RKKY interactions depend on a, this typical range of lattice parameters turns out to favor AFM ground states and/or fluctuations in these systems, including all the compounds cited above.

Nevertheless, RKKY interactions are also oscillatory in $2k_F a$, where k_F is the radius of the conduction electron Fermi surface. Thus, although rare, ferromagnetic (FM) ground states have been observed in the tetragonal Kondo compounds CeRu$_2$Ge$_2$, CeAgSb$_2$, CeZn$_{1-\delta}$Sb$_2$ and, more recently, CeRuPO and CePd$_2$P$_2$ [9–13]. In particular, intense efforts have been made to understand the unusual FM properties observed in CeAgSb$_2$, namely (i) larger magnetic susceptibility perpendicular to [001] ($\chi_\perp$) despite that the magnetic ordered moment below T_c is parallel to the c axis; (ii) linear increase of the hard-axis magnetization with magnetic field below T_c reaching $\sim 1.2 \mu_B$ at 3 T, a value much larger than the spontaneous moment along the c axis, 0.4 μ_B [14–16]. The origin of such intriguing properties has been elucidated by a combination of neutron scattering experiments and fits of χ to a Hamiltonian containing both CEF and anisotropic interactions terms [18]. The positive value of the CEF parameter B$_2^0$ accounts for $\chi_\perp > \chi_{||}$ and an exchange interaction with strong Ising character ($J_z \gg J_{x,y}$) drives the magnetic ordering of the z component of the angular momentum to take over the in-plane ordering. Moreover, an unexpected pure $|\pm 1/2\rangle$

ground state has been shown to be realized. Whether such an unusual CEF scheme is particular to CeAgSb$_2$ or a general trend of ferromagnetic members in the 112 system is still an open question.

In this context, we revisit the CeTX_2 family of compounds (T = transition metal, X = pnictogen) by studying and modeling the macroscopic properties of a novel member with T = Cd and X = Sb. As expected, CeCd$_{0.7}$Sb$_2$ is an intermetallic compound which crystallizes in the tetragonal ZrCuSi$_2$-type structure ($P4/nmm$ space group) with a stacking arrangement of CeSb-T-CeSb-Sb layers. As a result of its ferromagnetic order at T_c = 3.0 K, CeCd$_{0.7}$Sb$_2$ turns out to be an interesting avenue to study the evolution of FM in this family since the distance between Ce ions (a = 4.376 Å) is very close to the one found in CeAgSb$_2$ (a = 4.363 Å). Moreover, by taking into account recent reports on the CeTBi$_2$ family of antiferromagnetic compounds, in this work we are able to make a thorough comparison between several antimonide and bismuthide members [20–27].

To this end, here we report the physical properties of CeCd$_{0.7}$Sb$_2$ by means of magnetic susceptibility, electrical resistivity, and specific heat measurements. Our results reveal a soft FM order with large anisotropy ratio $\chi_\perp / \chi_{||}$ = 15 at T_c. A simultaneous analysis of both magnetization and specific heat data has been performed within the framework of mean field theory with anisotropic first-neighbor interactions, as well as the tetragonal CEF Hamiltonian. The best fits to our data yield the CEF scheme, as well the RKKY exchange parameters between Ce^{3+} ions. Interestingly, a pure $|\pm 1/2\rangle$ ground state doublet is obtained, exactly as in CeAgSb$_2$, suggesting a trend in the FM members. Our results also point out to a more general scenario where the dimensionality of the system, possibly given by the ratio c/a, induces a crossover from AFM to FM order accompanied by a drastic change of ground state.

II. EXPERIMENTAL DETAILS

Single crystals of CeCd$_{0.7}$Sb$_2$ with typical crystal sizes of $2 \times 2 \times 0.1$ mm^3 were grown from a combined Cd/Bi

flux. The crystallographic structure was verified by x-ray powder diffraction and the extracted lattice parameters are $a = 4.376(3)$ Å and $c = 10.903(5)$ Å. Although the value of a is very similar to the one obtained for CeAgSb$_2$ ($a = 4.363(1)$ Å and $c = 10.699(5)$ Å), the c parameter is 2% larger, likely associated with the lattice expansion due to the larger transition metal ion. In addition, several samples were submitted to elemental analysis using a commercial energy dispersive spectroscopy (EDS) microprobe, which revealed the stoichiometry to be 1:0.7:2 with an error of 5%. We note that deficiency at the transition metal site is a common trend in this family of compounds, as observed in CeZn$_{1-\delta}$Sb$_2$, CeAu$_{1-\delta}$Bi$_2$, CeNi$_{1-\delta}$Bi$_2$, and CeAu$_{1-\delta}$Sb$_2$, to name a few [11,26–28]. Nevertheless, in CeCd$_{0.7}$Sb$_2$ the magnetic transition observed at T_c is very sharp and both residual resistivity ($\rho_0 = 0.4\,\mu\Omega$cm) and residual resistance ratio (RRR = 76) are consistent with the properties of a good metal.

Magnetization measurements were performed using a superconducting quantum interference device (SQUID). The specific heat was measured using a small mass calorimeter that employs a quasiadiabatic thermal relaxation technique. The in-plane electrical resistivity was obtained using a low-frequency ac resistance bridge and a four-contact configuration.

III. RESULTS AND DISCUSSIONS

Figure 1(a) shows the temperature dependence of the magnetic susceptibility inverse, $\chi(T)^{-1}$, when a magnetic field of 1 kOe is applied parallel to the c axis, $\chi_{||}$, and perpendicular to it, $\chi_\perp$. As in CeAgSb$_2$, $\chi_\perp > \chi_{||}$ at high T, pointing out to an easy axis in the ab plane. The opposite behavior (i.e., $\chi_\perp < \chi_{||}$) is found in the AFM family CeTBi$_2$ and in the AFM antimonide members with $T =$ Au and Cu. Although CeAgSb$_2$ displays a Curie-like behavior at high T for both directions, $\chi_{||}$ data of CeCdSb$_2$ display a broad maximum related to CEF effects. The solid lines in Figs. 1 and 3(b) represent the best fits of the data to a CEF mean field model discussed below.

The inset of Fig. 1(a) displays the low temperature $\chi(T)$ data, which show a clear ferromagnetic (FM) transition at $T_c \simeq 3$ K and a magnetic anisotropy again consistent with an easy axis along the ab plane. The ratio $\chi_\perp/\chi_{||} \approx 15$ at T_c is mainly determined by the tetragonal CEF splitting and reflects the low-T Ce^{3+} single ion anisotropy. A Curie-Weiss fit to the polycrystalline averaged data for $T > 150$ K yields an effective magnetic moment $\mu_{\text{eff}} = 2.5(1)\,\mu_B$, in agreement with the theoretical value of $\mu_{\text{eff}} = 2.54\,\mu_B$ for Ce^{3+} (not shown). A paramagnetic Curie-Weiss temperature of $\theta_p = -24$ K is extracted, which is unexpected considering the FM order. We note that this value of θ_p is similar to the one found in the AFM series CeTBi$_2$. In a molecular field approximation, θ_p is proportional to the effective exchange interaction when CEF effects are neglected. Thus, a similar value of θ_p may indicate comparable effective exchange interactions at high temperatures, even though the magnetic ordered state is distinct. We also note that a negative value of θ was found in polycrystalline samples of CeZnSb$_2$, which recently has been shown to order ferromagnetically at $T_c = 3.6$ K [11,29].

Figure 1(b) displays the magnetization at 1.8 K as a function of magnetic fields applied parallel to the c axis $M_{||}$, and along the ab plane $M_\perp$. The large magnetic anisotropy of
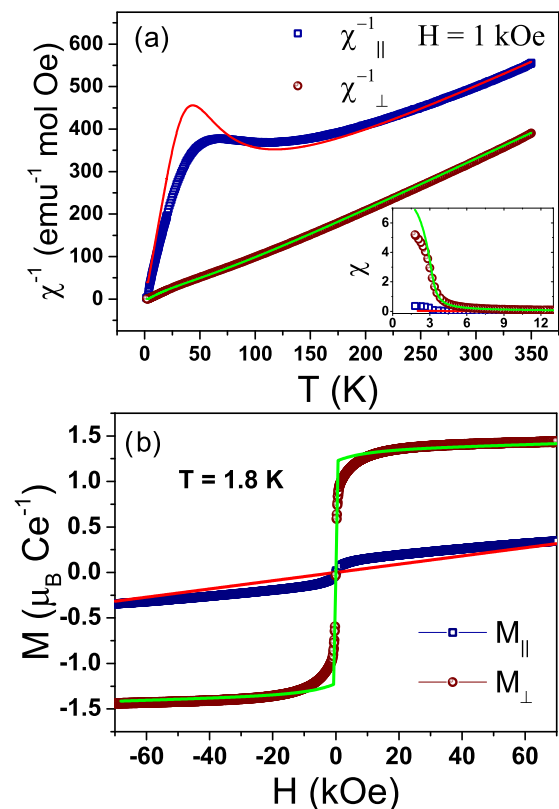

FIG. 1. (Color online) Temperature dependence of the inverse of the magnetic susceptibility measured with $H = 1$ kOe applied parallel ($1/\chi_{||}$) and perpendicular ($1/\chi_\perp$) to the c axis. The inset displays the low-T behavior of χ. (b) Magnetization as a function of the magnetic field applied perpendicular (open spheres) and parallel (open squares) to the c axis at $T = 1.8$ K. The solid lines through the data are best fits of the data using the CEF mean field model discussed in the text.

CeCd$_{0.7}$Sb$_2$ is also evident in this set of data where $M_\perp \gg M_{||}$. In particular, the saturation value for $M_\perp$ reaches 1.44 μ_B/Ce while the highest field value of $M_{||}$ reaches only 0.34 μ_B/Ce, indicating that the magnetization is far from saturation for $H||c$. Furthermore, low-field $M_\perp$ data display soft magnetic behavior with a coercive field $H_c = 36(3)$ Oe.

The in-plane electrical resistivity, $\rho_{ab}(T)$, of CeCd$_{0.7}$Sb$_2$ as a function of temperature is shown in Fig. 2. At high temperatures ($T > 150$ K), $\rho(T)$ decreases linearly with decreasing temperature. As the temperature is further decreased, a broad feature emerges centered at $\sim$125 K due to the thermal depopulation of the first excited CEF level. At $T_c = 3$ K, $\rho_{ab}(T)$ drops sharply as the magnetic scattering becomes coherent. A second kink at $T = 0.6$ K is observed in the low temperature data, as shown in the right inset of Fig. 2, which is likely due to a change in magnetic structure. In fact, it has been shown that CeZn$_{1-\delta}$Sb$_2$ undergoes a subsequent AFM transition at $T_N = 0.8$ K [11].

As in CeAgSb$_2$, we now try to fit $\rho_{ab}(T)$ of CeCd$_{0.7}$Sb$_2$ below T_c and above T_N to the expression:

$$\rho(T) = \rho_0 + AT^2 + D\frac{T}{\Delta}\left(1 + \frac{2T}{\Delta}\right)e^{-\Delta/T}. \quad (1)$$

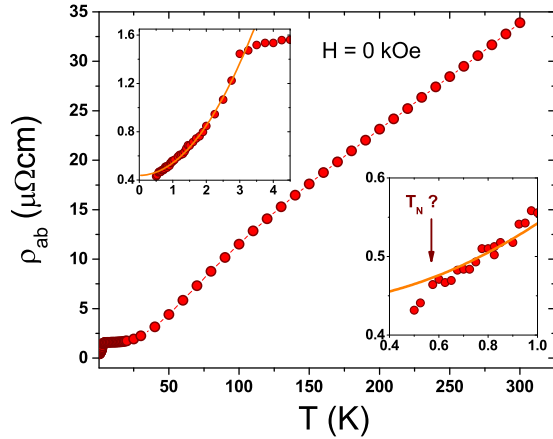The first two terms describe the usual Fermi-liquid (FL) expression. The third term is the contribution from an energy

FIG. 2. (Color online) Temperature dependence of the in-plane electrical resistivity ρ_{ab}. The left inset shows a fit to Eq. (1). The right inset displays the low temperature data.

gap in the magnon dispersion relation where D is related to the electron magnon and spin disorder scattering and Δ is the magnitude of the gap [30].

The best fit of the data to Eq. (1) (solid lines in the left inset of Fig. 2) yields a small residual resistivity of 0.4 $\mu\Omega$cm which, in addition to the relatively high residual resistivity ratio [RRR $\equiv (\rho_{300K} - \rho_{0.5K})/\rho_{0.5K}$] of 76, indicates good crystallinity and homogeneity despite the presence of Cd deficiency. Interestingly, both the coefficient D and the magnon gap Δ tend to zero, suggesting that the magnon contribution to the scattering is gapless. Hence, the T^2 term dominates and the extracted A coefficient is 0.1 $\mu\Omega$ cmK^{-2}, a value very close to the one found in CeAgSb$_2$ ($A = 0.07\,\mu\Omega$ cmK^{-2}). In CeAgSb$_2$, the Kadowaki-Woods (K-W) relation ($A/\gamma^2 = 1.7 \times 10^{-5}\,\mu\Omega$ cm(mol K/mJ)^2) has been used to obtain the linear γ coefficient. It is tempting to use the same expression to CeCd$_{0.7}$Sb$_2$ and obtain $\gamma = 77$ mJ/mol K^2, which in turn would indicate a moderately heavy fermion system. We note, however, that spin disorder in gapless ferromagnets may also give rise to T^2 resistivity [31,32]. Therefore, the K-W relation may not be valid in the present case.

To further explore the electronic contribution to the physical properties as well as the magnetic entropy associated with the FM order, we now turn our attention to specific heat measurements. Figure 3(a) shows the total specific heat divided by temperature, $C(T)/T$, as a function of temperature for CeCd$_{0.7}$Sb$_2$ (open triangles) and its nonmagnetic counterpart LaCd$_{0.7}$Sb$_2$ (solid line). Figure 3(b) presents the magnetic specific heat $C_{mag}(T)/T$ of CeCd$_{0.7}$Sb$_2$ after the subtraction of the lattice contribution from the La member. The clear peak of $C_{mag}(T)/T$ defines $T_c = 3$ K consistently with both magnetization and electrical resistivity data. The inset of Fig. 3(b) shows the magnetic entropy (S_{mag}) obtained by integrating $C_{mag}(T)/T$ over temperature. At T_c, $S_{mag} \sim 80\%$ of Rln2 and the entropy of the doublet is fully recovered at ~ 7 K. This reduction of S_{mag} at T_c may be due to two indistinguishable contributions, namely, a partial compensation of the Ce^{3+} CEF ground state due to the Kondo effect and magnetic frustration/short-range interactions due to competing magnetic interactions. In fact, a second transition occurs in $C_{mag}(T)/T$ at
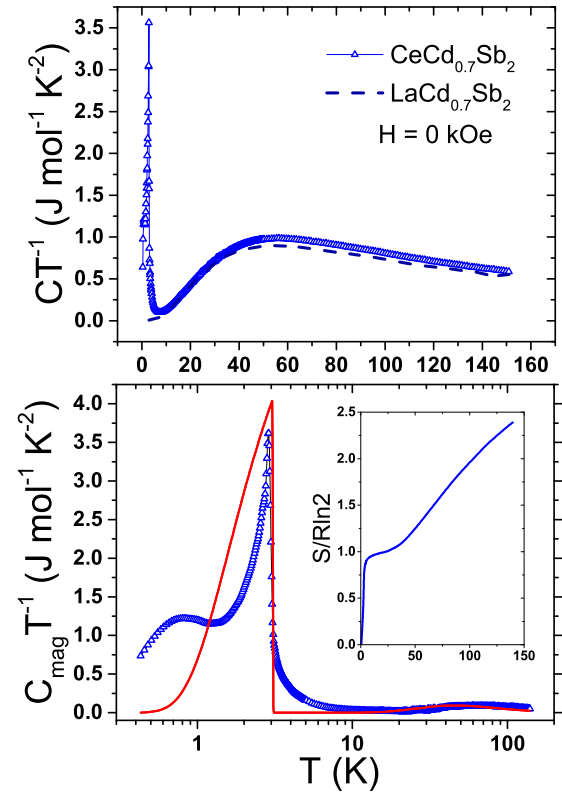

FIG. 3. (Color online) (a) $C(T)/T$ of CeCd$_{0.7}$Sb$_2$ and LaCd$_{0.7}$Sb$_2$ as a function of temperature. (b) $C_{mag}(T)/T$ vs T and the corresponding fit (solid line) using the model discussed in the text. The inset shows the magnetic entropy normalized by Rln2.

0.6 K, signaling for a change in magnetic structure. Moreover, the shoulder above 3 K suggests the presence of short-range interactions, which were not observed in CeAgSb$_2$ [19]. At high T, $C_{mag}(T)/T$ displays a broad feature due to the Schottky-type anomaly resulted from the CEF splitting of 125 K, as discussed below. In fact, S_{mag} at 125 K is Rln4, which includes the ground state and the first excited doublet. We note that, due to the successive magnetic ordering in CeCd$_{0.7}$Sb$_2$, an accurate estimate of γ at low temperatures is, unfortunately, not feasible. Moreover, the Schottky anomaly and short-range interactions prevent an estimate of γ in the paramagnetic state.

In order to establish a plausible scenario for the magnetic properties of CeCd$_{0.7}$Sb$_2$, we now analyze the data presented in Figs. 1 and 3(b) using a mean field model including two anisotropic interactions between nearest neighbors as well as the tetragonal CEF given by

$$\mathcal{H} = J_{AFM} \sum_{\langle i,l \rangle} j_i \cdot j_l + B_2^0 O_2^0 + B_4^0 O_4^0 + B_4^4 O_4^4, \quad (2)$$

where $J_{AFM} > 0$ represents an AFM interaction between nearest neighbor local spins j_i, B_i^n are the CEF parameters, and O_i^n are the Stevens equivalent operators obtained from the angular momentum operators [33,34]. For instance, the operator $O_{2,i}^0 = 3\hat{J}_{z,i}^2 - J(J+1)$ favors in-plane alignment of spins (i.e., $\hat{J}_z = 0$) if $B_{20} > 0$. Analogously, if $B_{20} < 0$ there is a tendency of alignment along the c axis. The Hamiltonian in Eq. (2) can be simplified to $zJj \cdot \langle j \rangle$ via mean field

TABLE I. Comparison between the extracted parameters (in Kelvin) for $CeCd_{0.7}Sb_2$ (this work), $CeAgSb_2$ [18], $CeCuBi_2$ [25], and $CeAu_{0.92}Bi_{1.6}$ [26]. Here, z_{AFM} (z_{FM}) are the Ce^{3+} nearest neighbors with an AFM (FM) coupling. In analogy to $CeCuBi_2$, where x-ray resonant magnetic scattering has been performed, $z_{AFM} = 2$ and $z_{FM} = 4$.

		CEF parameters (in Kelvin)				
Compound	Tc,N	B_2^0	B_4^0	B_4^4	$z_{FM}J_{AFM}$	$z_{FM}J_{FM}$
$CeCd_{0.7}Sb_2$	3 (FM)	12.3	-0.28	2.19	0.2	-1.1
$CeAgSb_2$	9 (FM)	7.6	-0.06	±0.7	-4	-47
$CeAu_{0.92}Bi_{1.6}$	12 (AFM)	-15.6	0.01	0.76	1.4	-1.1
$CeCuBi_2$	16 (AFM)	-7.67	0.18	0.11	1.1	-1.2

approximation ($j_i \cdot j_l \sim j \cdot \langle j \rangle$), where z is the number of nearest neighbors. Although $\mathcal{H}$ can be solved by this approach, the macroscopic properties of this family of compounds can be well fit only when we include a second ferromagnetic exchange interaction J_{FM}, indicating the presence of anisotropic RKKY interactions.

Hence, this model was used to simultaneously fit $\chi(T)$, $M(H)$, and $C_{mag}(T)/T$ data in the entire range of temperature. The best fits yield the CEF parameters and exchange interactions displayed in Table I, which are compared to previous analyses on $CeAgSb_2$, $CeAu_{0.92}Bi_2$, and $CeCuBi_2$ [17,18,25,26]. The first clear difference between these compounds is the sign of B_{20}, which is negative for AFM members and positive for FM members. According to the discussion above, this result indicates that in-plane alignment of spin is favored in FM compounds while c-axis alignment is favored in AFM compounds. In fact, it is known from previous x-ray magnetic resonant scattering measurements on $CeCuBi_2$ that its magnetic structure contains spins aligned along the c axis [25]. Moreover, the resolved magnetic structure shows a pattern (++−) with in-plane FM interactions and out-of-plane AFM interactions. In the ferromagnetic $CeAgSb_2$, $\chi\perp$ at higher temperatures is indeed larger than $\chi||$. However, due to the strong Ising character of the exchange interactions ($J_z \gg J_{x,y}$), the magnetic ordering of the z component $\hat{J}_z$ takes over the ordering of the in-plane components [18].

Table II displays the corresponding eigenfunctions and eigenvalues of $CeCd_{0.7}Sb_2$. The ground state is a pure $\Gamma_6 = |\pm 1/2\rangle$ doublet, exactly as in $CeAgSb_2$, followed by the first excited doublet $\Gamma_7^{(2)} (-0.47|\pm 5/2\rangle + 0.88|\mp 3/2\rangle)$ at 127 K,

TABLE II. Energy level and wave functions of the CEF scheme obtained from the thermodynamic properties of $CeCd_{0.7}Sb_2$.

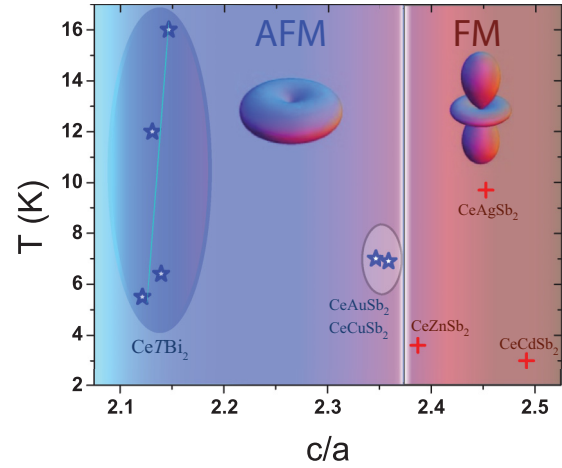|	Energy levels and wave functions					
$E(K)$	$|-5/2\rangle$	$|-3/2\rangle$	$|-1/2\rangle$	$|+1/2\rangle$	$|+3/2\rangle$	$|+5/2\rangle$
270	-0.88	0.0	0.0	0.0	-0.47	0.0
270	0.0	0.47	0.0	0.0	0.0	0.88
128	0.0	0.88	0.0	0.0	0.0	-0.47
128	-0.47	0.0	0.0	0.0	0.88	0.0
0	0.0	0.0	1.0	0.0	0.0	0.0
0	0.0	0.0	0.0	1.0	0.0	0.0

FIG. 4. (Color online) Magnetic ordering temperature vs lattice parameter ratio c/a for several members of the family $CeTX_2$. The ellipses in the AFM side enclose two distinct series of compounds: bismuthides (antimonides) for small (large) values of c/a. The cartoons on each side represent the charge distributions of the $4f$ electrons for the particular CEF ground state wave function: mainly $|5/2\rangle$ for AFM members and pure $|1/2\rangle$ for FM members.

and the second excited doublet $\Gamma_7^{(1)} (0.62|\pm 5/2\rangle + 0.78|\mp 3/2\rangle)$ at 270 K. The obtained CEF scheme and exchange constants, $z_{AFM} * J_{AFM} = 0.2$ K and $z_{FM} * J_{FM} = -1.1$ K, describe well the main features of the thermodynamic data shown in Figs. 1 and 3(b): the value of T_c, the magnetic anisotropy of $\chi(T)$, and the Schottky anomaly in $C_{mag}(T)/T$. However, it is important to notice that the CEF parameters obtained from fits to macroscopic measurements may not be as precise and unique. An accurate determination of the CEF scheme and its parameters does require a direct measurement by, for instance, inelastic neutron scattering [35], while the mixed parameters of the wave functions may be compared with an x-Ray absorption study [36].

Nonetheless, the analysis presented here clearly shows a trend in this family of compounds, as summarized in Fig. 4. For small values of the ratio c/a, T_N increases in the bismuthide series $CeTBi_2$ ($T =$ Ni, Ag, Au, and Cu). As c/a approaches the critical value of ~ 2.37, T_N starts to decrease, as found in the antimonides $CeAuSb_2$ and $CeCuSb_2$. When c/a is further increased through the AFM-FM border, T_c is observed in $CeZnSb_2$ at 3 K. Similarly to the AFM side, T_c first increases with increasing c/a and reaches a maximum value of 9 K in $CeAgSb_2$. Finally, as c/a is further increased, the FM order becomes unstable and T_c decreases in the member $CeCd_{0.7}Sb_2$.

These observations may be understood by taking into account the magnetic structure of $CeCuBi_2$, i.e., in-plane FM interactions and AFM interactions along the c axis. We first considered the case of FM members with similar lattice parameter a. In this simple case, the large values of c, in comparison with AFM members, imply that the inter-plane AFM exchange becomes unfavorable due to the substantial spacing between layers. In turn, the magnetic anisotropy is inverted ($\chi_\perp > \chi_\parallel$) and B_{20} changes sign. Finally, this rearrangement is reflected in the ground state which drastically changes from mainly $|\pm 5/2\rangle$ to pure $|\pm 1/2\rangle$, as shown by the cartoons of Fig. 4 [37]. More generally, the ground state

depends on the interplay between both lattice parameters. For instance, via the lattice parameter ratio c/a, which takes into account the dimensionality of the system. As shown in Fig. 4, c/a values ranging from 2.1 to 2.37 result in AFM order with ground state $|\pm 5/2\rangle$ and negative B_{20} values. For $c/a > 2.37$, FM ordering is favored with negative B_{20} values and a pure $|\pm 1/2\rangle$ ground state.

All the above arguments corroborate to the claim that the CeTX_2 family of compounds presents strong local moment magnetism with a moderate Kondo compensation. The weak hybridization between the Ce$^{3+}4f$ ions and the conduction electrons likely explains why this system is less propitious to host heavy fermion superconductivity, at least under ambient pressure. Our results also give a general scenario for the competing magnetic interactions commonly observed in these materials.

IV. CONCLUSIONS

In summary, we have studied temperature-dependent magnetic susceptibility, electrical resistivity, and heat capacity on CeCd$_{0.7}$Sb$_2$ single crystals. Our data reveal that CeCd$_{0.7}$Sb$_2$ orders ferromagnetically at $T_c = 3.0$ K and displays weak heavy fermion behavior. The detailed analysis of the macroscopic properties of CeCd$_{0.7}$Sb$_2$ using a mean field model as well as the tetragonal CEF suggest that the strongly localized Ce$^{3+}4f$ electrons are subjected to dominant CEF effects and anisotropic RKKY interactions. The extracted CEF scheme displays a pure $|\pm 1/2\rangle$ ground state, as found in the ferromagnet CeAgSb$_2$, hinting at a general trend within the ferromagnetic members. More generally, our results shed light on the magnetic anisotropy in this family of compounds and the role of dimensionality on the emergence of ferromagnetism.

[1] P. Misra, *Heavy-Fermions Systems* (Elsevier Science, New York, 2007).

[2] F. Steglich, J. Aarts, C. D. Bredl, W. Lieke, D. Meschede, W. Franz, and H. Schafer, Phys. Rev. Lett. **43**, 1892 (1979).

[3] H. Hegger, C. Petrovic, E. G. Moshopoulou, M. F. Hundley, J. L. Sarrao, Z. Fisk, and J. D. Thompson, Phys. Rev. Lett. **84**, 4986 (2000).

[4] C. Petrovic, P. G. Pagliuso, M. F. Hundley, R. Movshovich, J. L. Sarrao, J. D. Thompson, Z. Fisk, and P. Monthoux, J. Phys.: Condens. Matter **13**, L337 (2001).

[5] V. A. Sidorov, M. Nicklas, P. G. Pagliuso, J. L. Sarrao, Y. Bang, A. V. Balatsky, and J. D. Thompson, Phys. Rev. Lett. **89**, 157004 (2002).

[6] J. D. Thompson, and Z. Fisk, J. Phys. Soc. Japan **81**, 011002 (2012).

[7] S. M. Thomas, P. F. S. Rosa, S. B. Lee, S. A. Parameswaran, Z. Fisk, and J. Xia, arXiv:1508.05444.

[8] L. Balicas, S. Nakatsuji, H. Lee, P. Schlottmann, T. P. Murphy, and Z. Fisk, Phys. Rev. B **72**, 064422 (2005).

[9] S. Sullow, M. C. Aronson, and B. D. Rainford, and P. Haen, Phys. Rev. Lett. **82**, 2963 (1999).

[10] K. D. Myers, S. L. Budko, I. R. Fisher, Z. Islam, H. Kleinke, A. H. Lacerda, and P. C. Canfield, J. Magn. Magn. Mater. **205**, 27 (1999).

[11] T. Park, V. A. Sidorov, H. Lee, Z. Fisk, and J. D. Thompson, Phys. Rev. B **72**, 060410(R) (2005).

[12] V. H. Tran and Z. Bukowski, J. Phys.: Condens. Matter **26**, 255602 (2014).

[13] C. Krellner, N. S. Kini, E. M. Brüning, K. Koch, H. Rosner, M. Nicklas, M. Baenitz, and C. Geibel, Phys. Rev. B **76**, 104418 (2007).

[14] G. Andre, F. Bouree, M. Kolenda, B. Lesniewska, A. Oles, and A. Szytua, Physica B **292**, 176 (2000).

[15] M. Houshiar, D. T. Adroja, and B. D. Rainford, J. Magn. Magn. Mater. **140**, 1231 (1995).

[16] M. J. Thornton, J. G. M. Armitage, G. J. Tomka, P. C. Riedi, R. H. Mitchell, M. Houshiar, D. T. Adroja, B. D. Rainford, and D. Fort, J. Phys.: Condens. Matter **10**, 9485 (1998).

[17] T. Takeuchi, A. Thamizhavel, T. Okubo, M. Yamada, N. Nakamura, T. Yamamoto, Y. Inada, K. Sugiyama, A. Galatanu, E. Yamamoto, K. Kindo, T. Ebihara, and Y. Onuki, Phys. Rev. B **67**, 064403 (2003).

[18] S. Araki, N. Metoki, A. Galatanu, E. Yamamoto, A. Thamizhavel, and Y. Onuki, Phys. Rev. B **68**, 024408 (2003).

[19] Y. Inada, A. Thamizhavel, H. Yamagami, T. Takeuchi, Y. Sawai, S. Ikeda, H. Shishido, T. Okubo, M. Yamada, K. Sugiyama, N. Nakamura, T. Yamamoto, K. Kindo, T. Ebihara, A. Galatanu, E. Yamamoto, R. Settai, and Y. Onuki, Phil. Mag. B **82**, 1867 (2002).

[20] A. Thamizhavel, A. Galatanu, E. Yamamoto, T. Okubo, M. Yamada, K. Tabata, T. C. Kobayashi, N. Nakamura, K. Sugiyama, K. Kindo, T. Takeuchi, and R. Settai, and Y. Onuki, J. Phys. Soc. Japan **72**, 2632 (2003).

[21] M. H. Jung, A. H. Lacerda, and T. Takabatake, Phys. Rev. B **65**, 132405 (2002).

[22] H. Mizoguchi, S. Matsuishi, M. Hirano, M. Tachibana, E. Takayama-Muromachi, H. Kawaji, and H. Hosono, Phys. Rev. Lett. **106**, 057002 (2011).

[23] X. Lin, W. E. Straszheim, S. L. Budko, and P. C. Canfield, J. Alloys Comp. **554**, 304 (2013).

[24] C. B. R. Jesus, M. M. Piva, P. F. S. Rosa, and C. Adriano, and P. G. Pagliuso, J. Appl. Phys. **115**, 17E115 (2014).

[25] C. Adriano, P. F. S. Rosa, C. B. R. Jesus, J. R. L. Mardegan, T. M. Garitezi, T. Grant, Z. Fisk, D. J. Garcia, A. P. Reyes, P. L. Kuhns, R. R. Urbano, C. Giles, and P. G. Pagliuso, Phys. Rev. B **90**, 235120 (2014).

[26] C. Adriano, P. F. S. Rosa, C. B. R. Jesus, T. Grant, Z. Fisk, D. J. Garcia, and P. G. Pagliuso, J. Appl. Phys. **117**, 17C103 (2015).

[27] P. F. S. Rosa, C. B. R. Jesus, C. Adriano, Z. Fisk, and P. G. Pagliuso, J. Phys.: Conf. Ser. **592**, 012063 (2015).

[28] S. Seo, V. A. Sidorov, H. Lee, D. Jang, Z. Fisk, J. D. Thompson, and T. Park, Phys. Rev. B **85**, 205145 (2012).

[29] O. Sologub, K. Hiebl, P. Rogl, and O. Bodak, J. Alloys Compd. **227**, 40 (1995).

[30] N. H. Andersen, *Crystalline Electric Field and Structural Effects in f-electron Systems*, edited by J. E. Crow, R. P. Guertin, and T. W. Mihalisin (Plenum, New York, 1980), p. 373.

[31] I. Mannari, Prog. Theor. Phys. **22**, 335 (1959).

[32] T. Kasuya, Prog. Theor. Phys. **22**, 227 (1959).

[33] K. W. H. Stevens, Proc. Phys. Soc. A **65**, 209 (1952).

[34] P. G. Pagliuso, D. J. Garcia, E. Miranda, E. Granado, R. Lora Serrano, C. Giles, J. G. S. Duque, R. R. Urbano, C. Rettori, J. D. Thompson, M. F. Hundley, and J. L. Sarrao, J. Appl. Phys. **99**, 08P703 (2006).

[35] A. D. Christianson, E. D. Bauer, J. M. Lawrence, P. S. Riseborough, N. O. Moreno, P. G. Pagliuso, J. L. Sarrao, J. D. Thompson, E. A. Goremychkin, F. R. Trouw, M. P. Hehlen, and R. J. McQueeney, Phys. Rev. B **70**, 134505 (2004).

[36] T. Willers, Z. Hu, N. Hollmann, P. O. Körner, J. Gegner, T. Burnus, H. Fujiwara, A. Tanaka, D. Schmitz, H. H. Hsieh, H.-J. Lin, C. T. Chen, E. D. Bauer, J. L. Sarrao, E. Goremychkin, M. Koza, L. H. Tjeng, and A. Severing, Phys. Rev. B **81**, 195114 (2010).

[37] During the preparation of this manuscript, we found that a $|\pm 3/2\rangle$ ground state is realized in the antiferromagnetic member CeAgBi$_2$ [7]. Thus, both $|\pm 3/2\rangle$ and $|\pm 5/2\rangle$ ground states may be obtained in the AFM side of the phase diagram displayed in Fig. 4, although $|\pm 5/2\rangle$ seems to be more common in this family.